TOOL POINT RECEPTANCE VARIATION WITH SPINDLE-HOLDER-TOOL SELECTION

Tony Schmitz[1,2]
[1]Mechanical, Aerospace, and Biomedical Engineering
University of Tennessee, Knoxville
Knoxville, TN 37996, USA
[2]Energy and Transportation Science Division
Oak Ridge National Laboratory
Oak Ridge, TN 37830, USA

INTRODUCTION[1]

Modal analysis is applied to measure and model the structural dynamics of complex systems [1]. Because an important consideration in milling is the vibration behavior of the cutting tool during material removal, modal techniques are used to study machine-spindle-holder-tool combinations [2]. Important parameters for predicting milling vibration behavior, which can be stable (i.e., exhibits forced vibration only) or unstable (i.e., exhibits either self-excited or period-*n* bifurcations [3]), are the workpiece material, tool geometry, machining parameters, and structural dynamics [2, 4]. The workpiece material and tool geometry collectively define the relationship between the commanded chip geometry and the cutting force required to shear away the chip. This relationship may be parameterized in the form of a mechanistic cutting force model or the force may be predicted from the material's constitutive model using finite element analysis. The structural dynamics depend on the machine, spindle, holder, and tool combination, including the tool's extension length from the holder.

Because the tool point receptance (or frequency response function, FRF) is required to select stable machining parameters, identifying it for arbitrary machine-spindle-holder-tool assemblies is required. This may be achieved through modal testing techniques, such as impact testing where an instrumented hammer is used to apply the impulsive force input and a linear transducer (typically an accelerometer) is used to measure the corresponding response output. The receptance is the complex, frequency domain ratio of the output to the input. To reduce measurement time, Schmitz et al. derived receptance coupling substructure analysis (RCSA) for tool point FRF prediction [5-9].

This paper describes a case study of tool point receptances for 72 combinations obtained using three CNC machine tools, two holders, two collets, and six carbide rods. Measurement and prediction are completed for each combination. The measurements are performed using impact testing. Predictions are completed using RCSA, where models of the tool and holder are coupled to a measurement of spindle, again obtained by impact testing using a standard artifact. It is demonstrated that the tool point receptance depends not only on the tool and holder geometries, but also on the spindle receptances and the interactions between them. Effects of the tool point receptances on machining stability are presented.

RCSA

RCSA analytically couples receptance models for the holder and tool to a receptance measurement for the machine-spindle. The required steps are described in the following paragraphs. To begin, consider the tool and holder modeling.

The direct receptances for the free-free beam shown in Fig. 1 due to externally applied harmonic forces $f_1(t)$ and $f_2(t)$, applied at coordinates $x_1(t)$ and $x_2(t)$, and moments $m_1(t)$ and $m_2(t)$, applied at $\theta_1(t)$ and $\theta_2(t)$, are provided in Eq. 1. The corresponding cross receptances are shown in Eq. 2. (Note that the coordinates are

listed to consider *f* or *m* individually, unlike Eq. 3 which combines the effects). These receptances are used to represent the tool and holder sections prior to coupling.

$$x_1 = h_{11} f_1 \quad x_1 = l_{11} m_1 \quad x_2 = h_{22} f_2 \quad x_2 = l_{22} m_2$$
$$\theta_1 = n_{11} f_1 \quad \theta_1 = p_{11} m_1 \quad \theta_2 = n_{22} f_2 \quad \theta_2 = p_{22} m_2 \tag{1}$$

$$x_1 = h_{12} f_2 \quad x_1 = l_{12} m_2 \quad x_2 = h_{21} f_1 \quad x_2 = l_{21} m_1$$
$$\theta_1 = n_{12} f_2 \quad \theta_1 = p_{12} m_2 \quad \theta_2 = n_{21} f_1 \quad \theta_2 = p_{21} m_1 \tag{2}$$

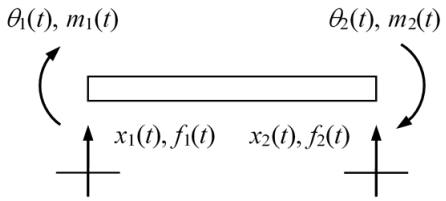

FIGURE 1. Free-free beam coordinates.

Equations 1 and 2 can be written in matrix form and compactly represented using the notation shown in Eq. 3.

$$\begin{Bmatrix} x_1 \\ \theta_1 \end{Bmatrix} = \begin{bmatrix} h_{11} & l_{11} \\ n_{11} & p_{11} \end{bmatrix} \begin{Bmatrix} f_1 \\ m_1 \end{Bmatrix} \text{ or } \{u_1\} = [R_{11}]\{q_1\}$$
$$\begin{Bmatrix} x_2 \\ \theta_2 \end{Bmatrix} = \begin{bmatrix} h_{22} & l_{22} \\ n_{22} & p_{22} \end{bmatrix} \begin{Bmatrix} f_2 \\ m_2 \end{Bmatrix} \text{ or } \{u_2\} = [R_{22}]\{q_2\} \tag{3}$$

In Eq. 3, R_{ij} is the generalized receptance matrix that describes both translational and rotational component behavior. The individual entries in these matrices include contributions from both the rigid body and flexural modes. In this study, the frequency dependent entries were calculated using the Timoshenko beam model, which includes the effects of rotary inertia and shear. It was implemented using finite elements [8], where each four degree-of-freedom (rotation and displacement at each end) free-free beam section was modeled using appropriate mass and stiffness matrices.

These receptances can be used to couple components at their end points in order to predict assembly dynamics. For example, a free-free beam with diameter d_1 can be coupled to a second free-free beam with larger diameter d_2 to synthesize the receptances for a stepped shaft (see Fig 2). The assembly flexural receptances, shown in Eq. 4 (the upper case variables denote assembly coordinates, forces, moments, and receptances), are determined by first writing the component displacements/rotations; see Eq. 5.

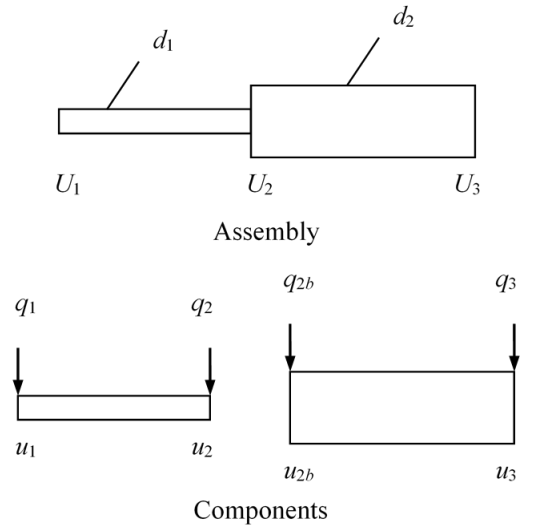

FIGURE 2. Stepped shaft assembly (top) and components (bottom). Diameters d_1 and d_2 are identified in the assembly schematic.

$$\begin{Bmatrix} U_1 \\ U_2 \\ U_3 \end{Bmatrix} = \begin{bmatrix} G_{11} & G_{12} & G_{13} \\ G_{21} & G_{22} & G_{23} \\ G_{31} & G_{32} & G_{33} \end{bmatrix} \begin{Bmatrix} Q_1 \\ Q_2 \\ Q_3 \end{Bmatrix} \text{ where } U_i = \begin{Bmatrix} X_i \\ \Theta_i \end{Bmatrix},$$
$$G_{ij} = \begin{bmatrix} H_{ij} & L_{ij} \\ N_{ij} & P_{ij} \end{bmatrix}, \text{ and } Q_i = \begin{Bmatrix} F_i \\ M_i \end{Bmatrix} \tag{4}$$

$$u_1 = R_{11} q_1 + R_{12} q_2 \qquad u_2 = R_{21} q_1 + R_{22} q_2$$
$$u_{2b} = R_{2b2b} q_{2b} + R_{2b3} q_3 \qquad u_3 = R_{32b} q_{2b} + R_{33} q_3 \tag{5}$$

For this stepped shaft example, a rigid connection is applied at the interface. The corresponding compatibility conditions are:

$$u_2 - u_{2b} = 0 \text{ and } u_i = U_i, \tag{6}$$

where i = 1 to 3 and the latter expression specifies that the component and assembly coordinates are defined at the same spatial positions. The equilibrium conditions vary with the external force/moment location. To determine the first column of the assembly receptance matrix in Eq. 4, Q_1 is applied to coordinate U_1. In this case, the equilibrium conditions are:

$$q_2 + q_{2b} = 0,\ q_1 = Q_1, \text{ and } q_3 = 0. \tag{7}$$

Substitution of the component displacements/ rotations and equilibrium conditions into the compatibility conditions yields q_2; see Eq. 8. The

expression for G_{11} is then given by Eq. 9. The other two first column receptances are determined in a similar manner. To find the receptances in the second and third columns, Q_2 must be applied to U_2 and Q_3 to U_3, respectively.

$$q_2 = -(R_{22} + R_{2b2b})^{-1} R_{21} Q_1 \tag{8}$$

$$G_{11} = \frac{U_1}{Q_1} = \frac{u_1}{Q_1} = \frac{R_{11}q_1 + R_{12}q_2}{Q_1}$$

$$G_{11} = R_{11} - R_{12}(R_{22} + R_{2b2b})^{-1} R_{21} = \begin{bmatrix} H_{11} & L_{11} \\ N_{11} & P_{11} \end{bmatrix} \tag{9}$$

In the case of finite stiffness and non-zero damping at the contact interface between components, the compatibility conditions can be modified to reflect the new coordinate displacement/rotation relationships. The Eq. 6 compatibility condition for the flexible-damped connection is now rewritten as:

$$K(u_2 - u_{2b}) = -q_{2b} \tag{10}$$

where the complex stiffness matrix is defined in Eq. 11 for a viscous damping model. In this matrix, the stiffness (k) and damping terms (c) are defined by their subscripts. The k_{xf} term, for example, describes the stiffness that relates force to displacement, while the stiffness $k_{\theta m}$ relates rotation to moment.

$$K = \begin{bmatrix} k_{xf} + i\omega c_{xf} & k_{\theta f} + i\omega c_{\theta f} \\ k_{xm} + i\omega c_{xm} & k_{\theta m} + i\omega c_{\theta m} \end{bmatrix} \tag{11}$$

Using the Eq. 10 compatibility condition, the assembly receptance from Eq. 9 is modified to be:

$$G_{11} = R_{11} - R_{12}(R_{22} + R_{2b2b} + K^{-1})^{-1} R_{21}. \tag{12}$$

For tool point receptance predictions, coordinates 1 and 2 in Eq. 12 are defined by the two ends of the holder-tool model, while coordinate 2b is associated with the machine-spindle. To experimentally identify the R_{2b2b} receptances, a standard artifact with the appropriate spindle-holder connection (e.g., CAT-40 or HSK-63A) is inserted in the spindle under test. The four direct receptances at the free end of the artifact are determined from a single displacement-to-force measurement as described in [9]. The machine-spindle receptances are then determined from the machine-spindle-artifact receptances using the inverse RCSA approach detailed in [8]. In this method, the assembly receptances are measured and then the free-free portion of the artifact beyond the holder flange is extracted to isolate the machine-spindle receptances; see Fig. 3.

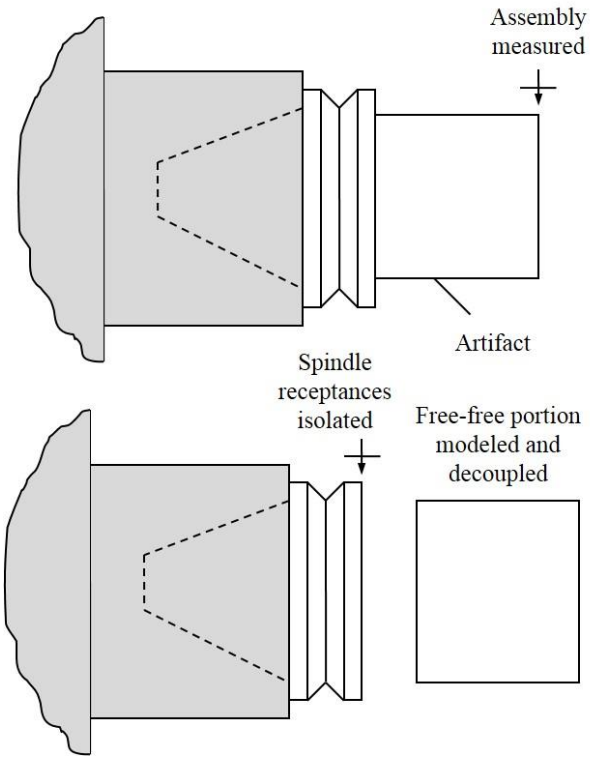

FIGURE 3. Machine-spindle receptances are determined using inverse RCSA.

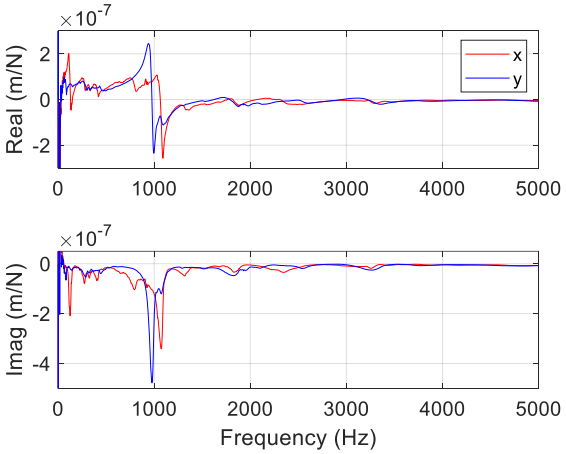

FIGURE 4. Haas TM1P machine-spindle receptances for the x and y directions.

RESULTS AND DISCUSSION

The RCSA approach was used to predict the tool point receptances for 72 machine-spindle-holder-tool combinations. This included three CNC machining centers: Haas TM1P, Haas VF5XT, and Makino a51nx; two collet holders: Parlec C40-32ER 312 and Parlec C40-32ER 412; two collets: ER32 12.7 mm and ER32 19.05 mm; and six carbide rods: 12.7 mm diameter, 77.01 mm long, 12.7 mm diameter, 102.62 mm long, 12.7 mm diameter, 127.36 mm long, 12.7 mm diameter, 152.72 mm long, 19.05 mm diameter, 76.24 mm long, 19.05 mm diameter, 153.26 mm long.

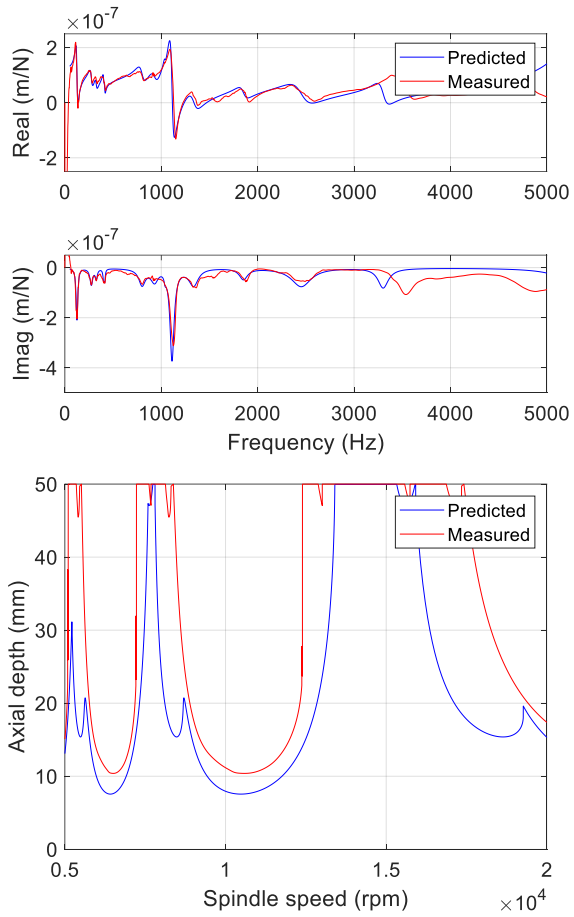

FIGURE 5. Haas TM1P: Parlec C40-32ER 312 holder with a 12.7 mm diameter, 77.01 mm long, 37 mm stickout carbide rod. (Top) Tool tip x receptances. (Bottom) Stability maps.

The first step was to determine the machine-spindle receptances for each of the three CNC machining centers using inverse RCSA. The artifact measurement the Haas TM1P (CAT-40 spindle-holder connection) is displayed in Fig. 4. Multiple vibration modes appear in the 5000 Hz measurement bandwidth. The measurements were completed using a PCB 086C03 modal hammer, PCB 352C23 low-mass accelerometer, and MLI's MetalMax TXF software. The portion of the cylindrical steel artifact beyond the flange was then extracted to isolate the machine-spindle receptances (see Fig. 3).

Tool tip measurements and predictions in the x direction for the Parlec C40-32ER 312 holder with a 12.7 mm diameter, 77.01 mm long, 37 mm stickout carbide rod are displayed in Figs. 5-7 for the three CNC machining centers. The associated stability maps are also included for 25% radial immersion down milling, 6061-T6 aluminum workpiece material, four teeth, and x direction feed. These are included to demonstrate the dramatic difference in stability behavior with changes in tool tip receptance from one machine to the next.

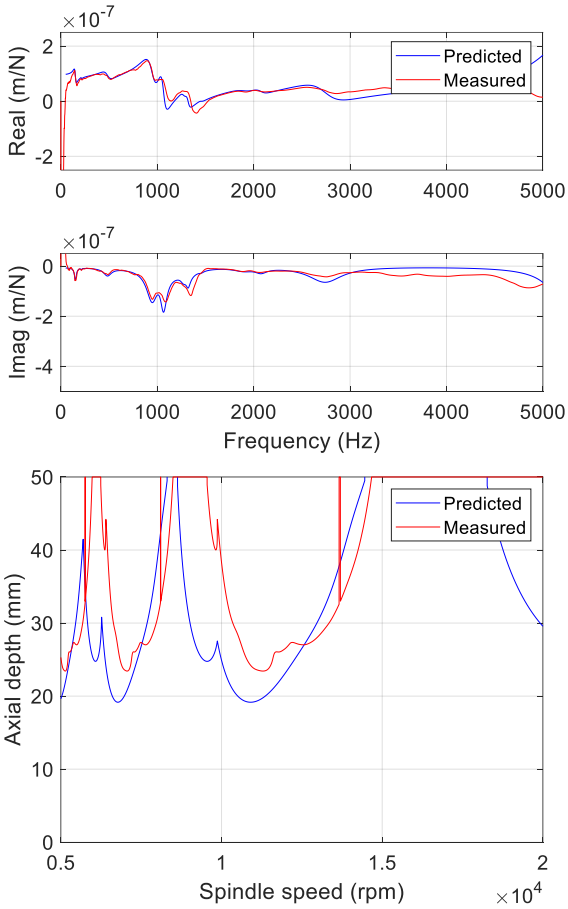

FIGURE 6. Haas VF5XT: Parlec C40-32ER 312 holder with a 12.7 mm diameter, 77.01 mm long, 37 mm stickout carbide rod. (Top) Tool tip x receptances. (Bottom) Stability maps.

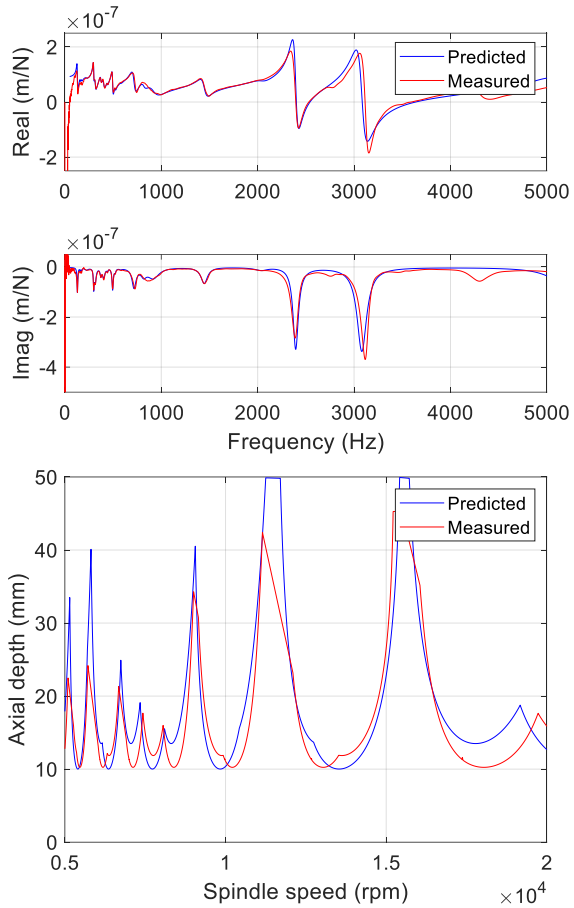

FIGURE 7. Makino a51nx: Parlec C40-32ER 312 holder with a 12.7 mm diameter, 77.01 mm long, 37 mm stickout carbide rod. (Top) Tool tip x receptances. (Bottom) Stability maps.

Figures 5-7 demonstrate a case where the tool length is short/stiff and the tool tip receptances therefore display multiple spindle-related modes. Figures 8-10, on the other hand, present the case where the tool length-to-diameter ratio is higher (so its stiffness is lower) and the tool's first bending mode dominates the tool tip receptance. Here, the y direction measurements and predictions for the Parlec C40-32ER 312 with a 19.05 mm diameter, 153.26 mm long, 113 mm stickout carbide rod are shown. It is interesting to note that the Makino a51nx result still includes interaction with spindle modes since there are spindle natural frequencies near the tool's first bending mode natural frequency.

CONCLUSIONS

This paper reported tool point receptance measurements and predictions for 72 machine-spindle-holder-tool combinations arranged using three CNC machine tools, two holders, two collets, and six carbide rods. The predictions were completed using receptance coupling substructure analysis (RCSA). The dependence of milling stability behavior on tool point receptance was demonstrated and it was seen that the same tooling inserted in a different spindle affects the milling performance.

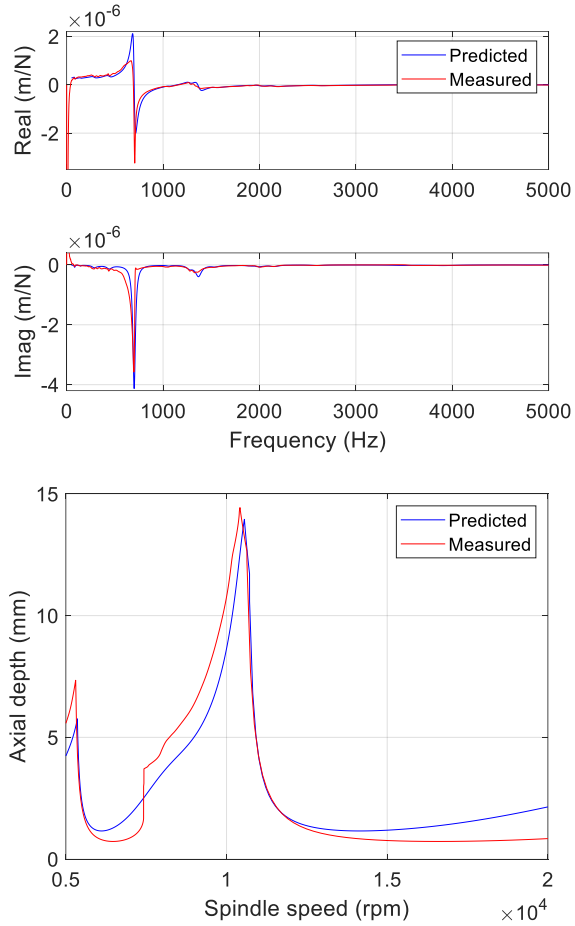

FIGURE 8. Haas TM1P: Parlec C40-32ER 312 holder with a 19.05 mm diameter, 153.26 mm long, 113 mm stickout carbide rod. (Top) Tool tip y receptances. (Bottom) Stability maps.

ACKNOWLEDGEMENTS

This research was supported by the National Science Foundation (CMMI-1561221) and DOE Office of Energy Efficiency and Renewable Energy (EERE), Energy and Transportation Science Division, and used resources at the Manufacturing Demonstration Facility, a DOE-EERE User Facility at Oak Ridge National Laboratory.

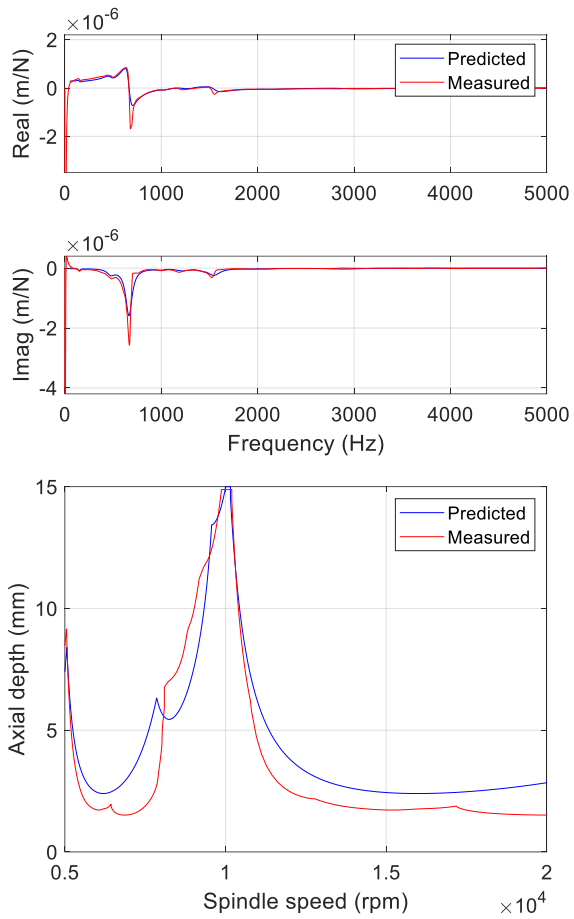

FIGURE 9. Haas VF5XT: Parlec C40-32ER 312 holder with a 19.05 mm diameter, 153.26 mm long, 113 mm stickout carbide rod. (Top) Tool tip y receptances. (Bottom) Stability maps.

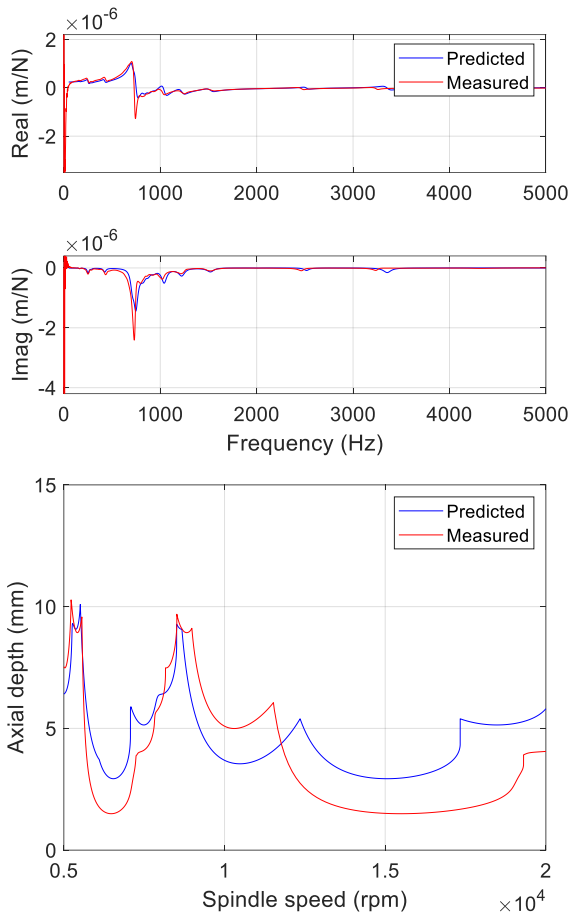

FIGURE 10. Makino a51nx: Parlec C40-32ER 312 holder with a 19.05 mm diameter, 153.26 mm long, 113 mm stickout carbide rod. (Top) Tool tip y receptances. (Bottom) Stability maps.

REFERENCES

[1] Ewins, D.J., 1984. Modal testing: Theory and practice (Vol. 15). Letchworth: Research Studies Press.

[2] Schmitz, T.L. and Smith, K.S., 2019. Machining dynamics: Frequency response to improved productivity, 2nd Ed. Springer, New York.

[3] Honeycutt, A. and Schmitz, T., 2018. Milling bifurcations: A review of literature and experiment. Journal of Manufacturing Science and Engineering, 140(12), 120801.

[4] Altıntaş, Y., 2000. Manufacturing automation. Cambridge University Press, New York.

[5] Schmitz, T.L. and Donaldson, R.R., 2000. Predicting high-speed machining dynamics by substructure analysis. CIRP Annals-Manufacturing Technology, 49(1), pp. 303-308.

[6] Schmitz, T.L., Davies, M.A. and Kennedy, M.D., 2001. Tool point frequency response prediction for high-speed machining by RCSA. Journal of Manufacturing Science and Engineering, 123(4), pp. 700-707.

[7] Schmitz, T.L., Davies, M.A., Medicus, K. and Snyder, J., 2001. Improving high-speed machining material removal rates by rapid dynamic analysis. CIRP Annals-Manufacturing Technology, 50(1), pp. 263-268.

[8] Schmitz, T.L. and Duncan, G.S., 2005. Three-component receptance coupling substructure analysis for tool point dynamics prediction. Journal of Manufacturing Science and Engineering, 127(4), pp. 781-790.

[9] Kumar, U.V. and Schmitz, T.L., 2012. Spindle dynamics identification for receptance coupling substructure analysis. Precision Engineering, 36(3), pp. 435-443.